# Calibrated Optical Time Transfer of UTC(k) for Supervision of Telecom Networks

Ł. Śliwczyński[1], P. Krehlik[1], J. Kołodziej[1],
H. Schnatz[2], D. Piester[2], A. Bauch[2], H. Imlau[3] and H. Ender[3]

[1]Faculty of Computer Science, Electronics and Telecommunications,
AGH University of Science and Technology, al. Mickiewicza 30, 30-059, Krakow, Poland
[2]Physikalisch-Technische Bundesanstalt (PTB), Bundesallee 100, 38116 Braunschweig, Germany
[3]Deutsche Telekom Technik GmbH, Neuenstraße 76-80, 28195 Bremen, Germany

## Abstract

We report on the evaluation of the performance of optical time transfer links connecting a facility of Deutsche Telekom in Bremen with the Physikalisch-Technische Bundesanstalt in Braunschweig. In the current configuration three links have been established, two via a hub in Hannover and one using an independent alternate route. They are equipped with electronically stabilized fiber optic time and frequency transfer systems and parallel operation is maintained since December 2016. A novel method of link calibration, composed of two steps (one performed in the laboratory and the second one in the field), to accurately determine the influence of fiber chromatic dispersion is discussed in detail, and a thorough analysis of the uncertainty budget is given. We show that the time transfer performance achieved is difficult to characterize based on measurements with time interval counters that are the standard equipment in timing laboratories and in the telecommunications sector. In our experiments, values of TDEV at the low ps-level at averaging times between $10^4$ to $10^6$ seconds have been achieved. The uncertainty of time transfer (including all kinds of delays) is of the order of 50 ps in a cascade of links. The results obtained show that such a kind of link is capable to deliver signals to a remote end with an instability being at least two orders of magnitude below the current requirements included in relevant Recommendations of the International Telecommunication Union – Telecommunication Sector (ITU-T). Moreover, the current implementation would allow primary Cs fountain clocks to be compared at the level of their performance, that is characterized by an uncertainty at the low $10^{-16}$ level and a frequency instability of the same order of magnitude at one day averaging.

**Keywords:** time transfer, frequency transfer, fiber optic, propagation delay calibration, uncertainty budget, telecom network supervision

## 1. Introduction

Nowadays telecommunication networks are complex systems used to convey a huge amount of data of various kinds into a large, multi-access infrastructure exploiting both mobile and stationary terminals. In order to assure data integrity over the entire network, a large number of network devices has to be synchronized to a common time reference.

Network synchronization chains of a telecom network (see Fig. 1 for an example) are built in a hierarchical way, with caesium clock-based so-called enhanced Primary Reference Time Clocks (ePRTC) at the top (called CORE level) from which signals are passed towards the lower hierarchy-level equipment. Requirements

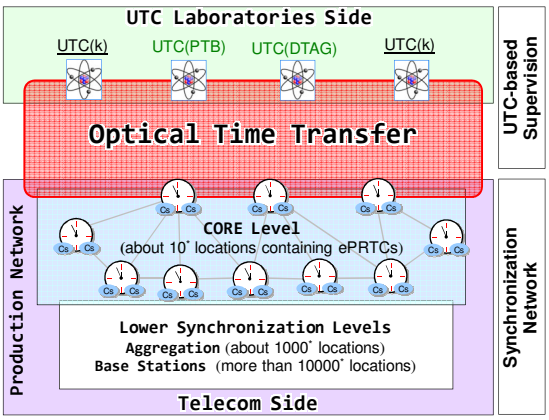


Fig. 1. Structure of possible telecommunication synchronization chain (numbers given are examples only and depend on the network size and topology).

concerning accuracy and stability of the synchronization chain levels are standardized in Recommendations issued by the International Telecommunication Union – Telecommunication Sector (ITU-T).

For routine operation of a so-called production network, techniques based on synchronous Ethernet (SyncE) and precision time protocol with full timing support (PTP-FTS) as described in the G.826x and G827x series of ITU-T Recommendations [1-3] should be sufficient. In particular, Recommendations G.8272 and G.8272.1 state that the network time should be traceable to a recognized international standard (e.g. Coordinated Universal Time UTC). In Germany, Deutsche Telekom Technik GmbH operates its timing center in Frankfurt/Main (DE) where a local realization of UTC, named UTC(DTAG), is maintained, and obtains traceability to UTC through the BIPM Circular T as many National Metrology Institutes (NMI).

The other option, often exploited in the telecom world, is to seek traceability by receiving signals from a global navigation satellite system (GNSS). Today the US Global Positioning System (GPS) is widely used in combination with Galileo and/or Glonass for this purpose. In this case, the question of traceability to UTC remains under debate [4-5]. Maybe even more important seems the fact that jamming/spoofing of satellite signals remains a continuous threat that is out of control of a telecom operator [6].

The requirements concerning the accuracy and stability of the synchronization chain levels are under continuous evolution in ITU-T Study Group 15, in view of the future needs for more accurate and more robust network synchronization. The nearest future 5$^{th}$ generation (5G) mobile telecom standard that is about to be rolled-out will use many specific techniques to increase the network throughput or spectral efficiency of radio interfaces. These include e.g. time domain duplex (TDD) operation, enhanced inter-cell interference cancellation (eICIC) functions, future new mobile location-based services including accurate geo-positioning for emergency calls, single-frequency network-based multi- and broadcast applications (MBSFN), and ultra-reliable low latency communication (URLLC). For their proper operation both frequency syntonization and time synchronization within a network become critical and the network operators must be prepared to support these technologies and operate them reliably. While 4G mobile technology has required a network synchronization better than 1.5 µs for all base stations at the air interface, 5G technology will require a level of synchronization by a factor of 10 more accurate. This is especially important for a service like URLLC.

The continuously growing requirements concerning synchronization of telecom networks spurred the idea to extend the standard synchronization topology by adding one more level to the usual hierarchy that would be responsible for supervision of critical synchronization network nodes. This would allow a network operator to continuously monitor the performance of ePRTCs independent of the network operations, as well as to detect and react on possible synchronization malfunction, increasing this way the reliability of the entire network. The time/frequency (T/F) technology used at this supervision level should necessarily outperform GNSS-based techniques. That naturally suggested consideration of optical fiber-based methods that have been extensively developed recently and exploited in numerous experiments, involving clock comparisons and frequency dissemination in both the optical [7-10] and the radio frequency (RF) domain [11-17]. Dedicated methods have been proposed allowing dissemination of time markers to remote users [18-22], but the same technology would allow accurate comparisons of clocks at two sites to be made.

The Physikalisch-Technische Bundesanstalt (PTB), Deutsche Telekom Technik GmbH, and AGH University of Science and Technology have collaborated in the field of synchronization of telecom networks by running jointly a series of proof of concept (PoC) experiments [26]. This paper is aimed to describe the most recent optical time transfer (OTT) installation (Section 2) and to report on its performance in the period between 2016 and 2018. Focus is laid on the aspect of ensuring time accuracy between the reference provided at the local terminal and the output at the remote terminal. The generic term “link calibration” is used for the several steps of measuring or calculating the propagation delays involved. We present here a novel method of determining the asymmetry of signal propagation through the fiber caused by chromatic dispersion, which, when compared to the method that had been described in our previous paper [27], is able to consider the effects related to lasers frequency chirping, and does not require the knowledge about the wavelengths difference of the lasers involved. This novel method will be detailed in Section 3, together with the corresponding uncertainty budget. In Section 4 we will present the results of two calibration campaigns that validates the proposed calibration procedure, whereas the transfer stability (including results of a 150 days long-term measurement campaign) will be discussed in Section 5.

## 2. Description of OTT infrastructureand equipment involved

To assess the benefits and advantages of OTT for the needs of a telecom operator, starting from July 2015, a number of PoC links have been established over the dark fibers owned by Deutsche Telekom Technik GmbH. After successful initial experiments related mainly to the long-term transfer reliability and stability through the plenitude of patched dark fibers of quite different production and roll-out times[26], the infrastructure has been upgraded in December 2016. As of today, five independent delay-stabilized T/F links (denoted using roman numbers from I to V and illustrated in Fig. 2) are operated, connecting PTB in Braunschweig (where UTC(PTB)

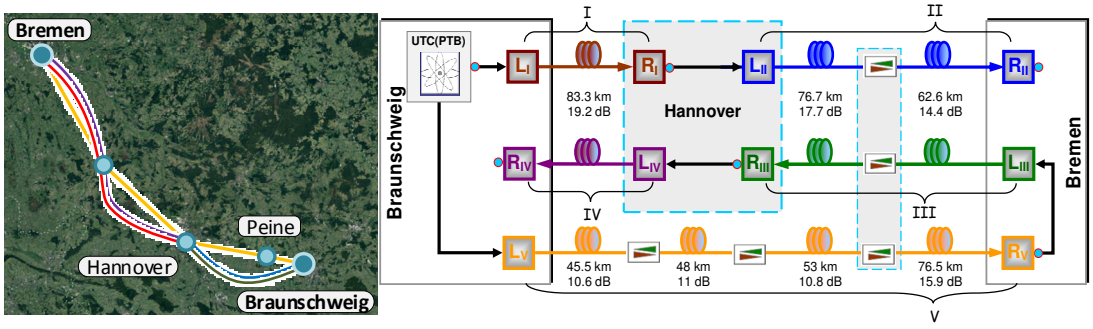


a) b)

Fig. 2. Current PoC OTT links: geographical localization (a) and logical connections (b).

is maintained) with telecom facilities in Hannover and Bremen. In Hannover, a T/F hub has been created. Signals arriving from PTB via link I are transmitted to Bremen via link II, signals from Bremen (via III) are routed back to PTB (via IV). From this hub the signals will in near future be routed to the Frankfurt facilities and at a later stage also to the Berlin facilities of Deutsche Telekom Technik GmbH. One immediate objective is to establish the OTT-based comparison between UTC(PTB) and UTC(DTAG), which is maintained in Frankfurt/Main. The link V includes additional amplifiers in Peine, between Braunschweig and Hannover, and it is routed through a separate Telekom facility in Hannover.

Each individual link is equipped with the ELSTAB fiber optic time (1 PPS) and frequency (10 MHz) transfer system with active fiber delay stabilization [22-23], and a number of single-path bi-directional optical amplifiers (SPBA) used to compensate for the fiber losses [24]. ELSTAB technology uses an intensity-modulated light that conveys T/F signals between the local and remote modules in both directions over the same optical fiber. Thanks to the symmetry of the propagation conditions and exploiting a feedback loop, the delay of both transmitted 1 PPS and 10 MHz signals can be stabilized at the output of the remote module. The specially designed matched electronic delay lines, manufactured as an application specific integrated circuit (ASIC), work as an active stabilization element with the range of delay change adequate for links up to about 100 km long [22]. In combination with additional optically switched delay banks this distance can be extended up to 1000 km [23]. The wavelengths of the lasers used to send lights in the counter propagating directions are stabilized against an external Fabry-Perot etalon and separated by an offset of 100 GHz to avoid limitations caused by Rayleigh backscattering[24].

The currently operated PoC OTT links provide the unique opportunity of performing extensive experimental tests and verifications thanks to the redundant topology. These activities included validation of our calibration procedures and the evaluation of the stability of the signals delivered to Bremen over two physically different fiber routes (links I+II and link V, respectively, see Fig. 2b).

## 3. Link calibration

To fully calibrate all described PoC OTT links it is necessary to calibrate each individual connection and consider the propagation delays caused by the connection between links V + III in Bremen and links I + II and III +IV in Hannover.

A simplified timing model illustrating the propagation of a1 PPS signal across one individual connection is shown in Fig. 3, where this link is considered as part of an installation transferring UTC(k) (left) to a remote user (right). The delay is stabilized between the reference point in the local module (1 $PPS_{REF}$) and the internal output point of the remote module marked with Ⓟ. The PPS advancing block allows coarse (with 10 ns resolution) compensation of the propagation delay introduced by the transfer system and thereby aligning the 1 PPS pulse at

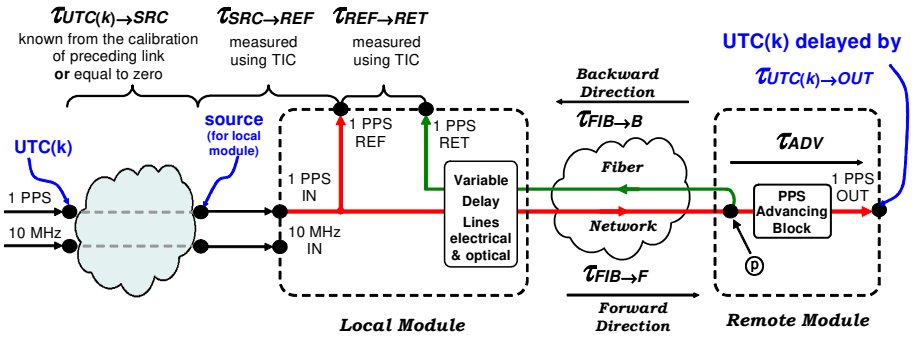


Fig. 3. Simplified timing model used for calibration of an individual link

the output of the remote module (1 $PPS_{OUT}$) to UTC(k) [28].

The propagation delay $\tau_{REF\to OUT}$ between the reference point (1 $PPS_{REF}$) of a local module and the output 1 $PPS_{OUT}$ of the remote module of the link can be expressed as:

$$\tau_{REF\to OUT} = \left(\tau_{REF\to RET} + \Delta\tau_{F\leftrightarrow B} + \tau_C\right)/2 - \tau_{ADV}\,, \tag{1}$$

where $\tau_{REF\to RET}$ is the round-trip delay between the 1 $PPS_{REF}$ and 1 $PPS_{RET}$ outputs of the local module. It is measured using a time interval counter (TIC) or equivalent instrument. $\tau_{ADV}$ represents an additional 1 PPS delay (positive or negative) set by the user. The remaining terms characterize the propagation delay asymmetry between the forward and backward directions: $\tau_C$ is a hardware-specific calibration value (which needs to be determined separately for each pair of local and remote modules during their manufacturing) whereas $\Delta\tau_{F\leftrightarrow B}$ is the correction factor related to the asymmetry of the optical fiber path. $\Delta\tau_{F\leftrightarrow B}$ can be further decomposed into a few terms:

$$\Delta\tau_{F\leftrightarrow B} = \tau_{\Delta\lambda} + \tau_S + \tau_B\,, \tag{2}$$

where $\tau_S$ and $\tau_B$ are related to the Sagnac effect and to the fiber polarization mode dispersion (PMD), respectively. The term $\tau_{\Delta\lambda}$ results from the intentional detuning $\Delta\lambda_{F\leftrightarrow B} = \lambda_F - \lambda_B$ of the wavelengths of the two lasers in the local and remote modules (denoted as $\lambda_F$ and $\lambda_B$, respectively) and the fiber chromatic dispersion:

$$\tau_{\Delta\lambda} = D_T \cdot \Delta\lambda_{F\leftrightarrow B}\,, \tag{3}$$

where $D_T = D\cdot L$ is the total dispersion accumulated over the fiber of length $L$, and $D$ is the fiber chromatic dispersion coefficient. In principle, $\tau_{\Delta\lambda}$ can be obtained directly from equation (3). This, however, requires accurate knowledge about the laser wavelength difference and about the accumulated chromatic dispersion at the specific wavelength of transfer system operation. Instead it is more adequate to measure $\tau_{\Delta\lambda}$ during link installation in situ. The method developed for this purpose and implemented in ELSTAB system is based on varying the wavelength of the laser in the local module [29].

### 3.1 Determining $\tau_{\Delta\lambda}$

The utilized method is based on a two-step procedure. In the first step, an initial pre-calibration of the link is performed in the laboratory using a test fiber link. Assuming that the laser in the local module changes its wavelength by $\Delta\lambda_{FM①}$ around its nominal value $\lambda_F$ (see Fig. 4) and that the delay compensating circuitry is deactivated, one will observe an associated change of the delay between 1 $PPS_{RET}$ and 1 $PPS_{REF}$ outputs of $\tau_{M①}$, where ① has been used to denote the first calibration step performed in the laboratory. Using this result, a value of $\tau^I_{\Delta\lambda①}$ can be determined indirectly (thus marked with $I$ in the superscript):

$$\tau^I_{\Delta\lambda①} = \tau_{M①}\frac{\Delta\lambda_{F\leftrightarrow B①}}{\Delta\lambda_{FM①}}\cdot S_①\,, \tag{4}$$

where $S_①$ is a correction factor that accounts for a slight dependence of the fiber chromatic dispersion on the wavelength (called dispersion slope).

For this value to be perfectly correct one would need to know the exact values of $\Delta\lambda_{F\leftrightarrow B①}$ and $\Delta\lambda_{FM①}$. This requirement, however, may be removed because both local and remote modules are collocated during this step and one is able to determine $\tau^R_{\Delta\lambda①}$, i.e. the required (thus marked with $R$ in the superscript) value that will satisfy equation (2) for the specific values used in this calibration step, by measuring directly the delays

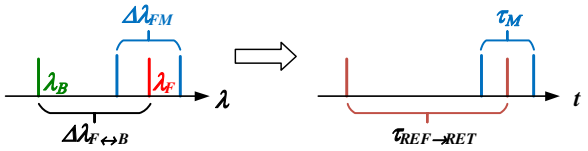


Fig. 4. An illustration of the principle of determining $\tau_{\Delta\lambda}$: assuming that the stabilizing loop is de-activated the change of the forward laser wavelength of $\Delta\lambda_{FM}$ results in corresponding change of $\tau_{REF\to RET}$ equal to $\tau_M$.

$\tau_{REF\to OUT①}$ and $\tau_{REF\to RET①}$:

$$\tau^{R}_{\Delta\lambda①} = 2\tau_{REF\to OUT①} - \tau_{REF\to RET①} - \tau_{C①}, \tag{5}$$

Prior to performing these measurements, the delay stabilization has to be activated again. Using (4) and (5), a correction factor $\Gamma$ can be determined as a result of the first step of measuring $\tau_{\Delta\lambda}$:

$$\Gamma = \frac{\tau^{R}_{\Delta\lambda①}}{\tau^{I}_{\Delta\lambda①}}. \tag{6}$$

The second step is performed during the installation of the transfer system connected by the target fiber, where the local and remote modules are placed in different locations. To determine the asymmetry of this particular fiber connection (the length of which will be usually different from the length of the fiber used in the first step in the laboratory), the procedure of varying the wavelength of the laser in the local module has to be repeated. Based on equations (4) and (6), its result can be stated as:

$$\tau^{I}_{\Delta\lambda②} = \Gamma\,\tau_{M②}\,\frac{\Delta\lambda_{F\leftrightarrow B②}}{\Delta\lambda_{FM②}}S_{②}, \tag{7}$$

where the symbol ② denotes that the values used come from the second step of determining $\tau_{\Delta\lambda}$.

Combining equations (4), (6) and (7) we finally achieve the equation:

$$\tau^{I}_{\Delta\lambda②} = \tau^{R}_{\Delta\lambda①}\cdot\frac{\Delta\lambda_{F\leftrightarrow B②}}{\Delta\lambda_{F\leftrightarrow B①}}\cdot\frac{\Delta\lambda_{FM①}}{\Delta\lambda_{FM②}}\cdot\frac{S_{②}}{S_{①}}\cdot\frac{\tau_{M②}}{\tau_{M①}}, \tag{8}$$

that allows determining the forward-backward asymmetry due to detuning of the lasers in the local and remote modules and chromatic dispersion of the fiber. Ideally, the equalities $\Delta\lambda_{F\leftrightarrow B①} = \Delta\lambda_{F\leftrightarrow B②}$ and $\Delta\lambda_{FM①} = \Delta\lambda_{FM②}$ will hold so that $\tau^{I}_{\Delta\lambda②}$ will not depend on these particular values as they cancel in equation (8). This form of equation, however, will be useful to estimate the uncertainty of the time transfer calibration that will be explained in Section 3.3.

Yet another reason justifying the use the correction factor $\Gamma$ is the fact that the laser pulses (which are used by ELSTAB to convey T/F information [22]) traveling along a dispersive fiber undergo distortions that depend on the characteristics of the laser, especially on its wavelength chirping. We observed that this could introduce some small asymmetry between the forward and backward directions because laser parameters are usually slightly different. Thanks to the laboratory pre-calibration in step ① this asymmetry can be taken into account.

### 3.2 Calibration of cascaded links

In case of cascaded links, equation (1) has to be extended to reflect the total delay from the UTC reference point to the output of a particular link (see Fig. 3). One of these delays, designated as $\tau_{SRC\to REF}$, represents the propagation of the signal from its local source for the particular link, whereas the second one $\tau_{UTC(k)\to SRC}$ represents the delay between the UTC(k) reference point and the local source. For the first link in the cascade, the local source is equivalent to the UTC(k) reference point, so $\tau_{UTC(k)\to SRC} = 0$. For the next link in the cascade $\tau_{UTC(k)\to SRC}$ is determined based on the calibration of the preceding link. With the two additional delays the complete form of equation showing the total delay is thus:

$$\tau_{UTC(k)\to OUT②} = \tau_{UTC(k)\to SRC②} + \tau_{SRC\to REF②} + \left[\tau_{REF\to RET②} + \Delta\tau_{F\leftrightarrow B②} + \tau_{C①}\right]\Big/2 - \tau_{ADV②}. \tag{9}$$

Going back to Fig. 2 that shows the entire PoC OTT links involved, it becomes obvious that performing their full calibration is quite a complex and time-consuming process that had to be performed in a targeted order. Calibration of each individual link requires accessing its local terminal, so starting from Braunschweig links I and V were calibrated. In the next step, link II was calibrated while working in Hannover. To set the value of $\tau_{ADV}$ for link IV, however, it was necessary to know the delay of the link III first, which could be determined only while working in Bremen. The value of $\tau_{ADV}$ was determined only after having made all necessary calibration measurements in Bremen. It was set remotely at a convenient time.

### 3.3 Calibration uncertainty

When analyzing the uncertainty of time transfer in the PoC OTT links, it is necessary to consider the propagation of uncertainties of individual links in cascaded operation. In addition, due to the specific method

used to determine $\tau^{I}_{\Delta\lambda②}$ described in Section 3.1, the two steps of calibration (step ① in the laboratory and step ② during installing the link over the target fiber), which are typically separated in time, makes the entire procedure sensitive to the long-term instability of the wavelengths of the lasers.

Equations (1), (2), (8) and (9) reveal that the uncertainty of time transfer depends on many factors, however the most important ones are related to the uncertainty of time interval measurement, the uncertainty of determining $\tau_{ADV②}$, $\tau^{R}_{\Delta\lambda①}$, and the potential instability of the wavelengths of the lasers in the local and remote modules. In addition, some difference of temperatures can be anticipated between steps ① and ②.

The measurements of time intervals are usually done using a differential method to avoid systematic errors of the equipment used. We used high-speed digital oscilloscopes (Agilent DSO81004A and DSO81004B in the 2016 and 2017 campaigns, respectively) and its histogram analysis option to make most of time interval measurements. Only a few measurements in PTB during the 2016 campaign were made using a Stanford Research SR620 TIC.

In our method the time interval is estimated as a mean value of the histogram that reduces the random component of the measurement uncertainty (jitter) with the square root of the number of waveforms used to assemble the histogram. Usually we use at least 20 waveforms for this purpose that makes the type A uncertainty less than 1 ps (one-shot noise is ~3 ps). So, it is negligible compared to the type B uncertainty of time interval measurements using the oscilloscope, resulting mainly from the inaccuracy of its time base. To mitigate this we exploited a special setup, where the oscilloscope is used only to measure the residual part of time interval, limited to less than 10 μs. In this setup, a highly-accurate 10 MHz signal (see details in Section 4) was used to generate 1 PPS pulses that are then delayed by a specific number of 10 MHz periods using a high-speed digital circuitry. This delay gives the information about the main part of the measured time interval. Based on the specifications of the oscilloscope, we estimated the standard uncertainty of such differential measurements to be in the range from 3.5 ps to 7 ps, depending on the time interval measured. In further analysis we used conservatively $u(\tau) = 7$ ps for any measurement performed using an oscilloscope.

The uncertainty of $\tau_{ADV②}$ includes some random component (type A) and nonlinearity (type B), both dependent to some extent on the value of the advance set. Laboratory measurements showed that the root-mean-square (RMS) of the jitter does not exceed 3 ps, whereas the nonlinearity is within the interval of ±1.5 ps [28]. The method described in the above paragraph allows once again to neglect the random uncertainty component – in further calculations we used a conservative value of $u(\tau_{ADV②}) \approx 2$ ps.

The uncertainty that can be attributed to $\tau^{R}_{\Delta\lambda①}$ results from equation (5). This includes two contributions, related to the measurements of time interval and the uncertainty related to determining the hardware calibration constant $\tau_{C①}$. This latter one reflects mainly the mismatch of the two delay lines used in the ELSTAB local module to stabilize the propagation delay. The mismatch value is characterized separately for each particular chip before its installation inside the ELSTAB system. Based on measurements done on several of such chips, the standard uncertainty $u(\tau_{C①})$ can be estimated as about 6.5 ps. This value is a bit smaller than used previously [27] because of various improvements of the ASIC's design.

Thanks to the laboratory calibration during step ①,the particular values of $\Delta\lambda_{F\leftrightarrow B}$ and $\Delta\lambda_{FM}$ appear in calibration formulas only as ratios. Any change of these values between steps ① and ②, however, will affect the uncertainty of determining $\tau^{I}_{\Delta\lambda②}$ as one can assume that in general $\Delta\lambda_{②} = \Delta\lambda_{①} + \varepsilon$, where $\varepsilon$ is the wavelength change. In ELSTAB we use external Fabry-Perot etalons to stabilize the lasers' wavelengths. Based on our experience with the design of the wavelength stabilization circuits with such etalons and of performed laboratory measurements, we can estimate the peak-to-peak fluctuations of laser wavelengths as about ±2 pm, that corresponds to a standard uncertainty $u(\Delta\lambda) \approx 1.2$ pm assuming uniform distribution.

After having performed step ② of calibration, the link starts its regular operation where the propagation delay of the individual link might undergo some small variations due to a residual change of the fiber chromatic dispersion and long-term instability of lasers wavelengths. These effects can be included in the uncertainty analysis by writing $\tau^{I}_{\Delta\lambda}$ as:

$$\tau^{I}_{\Delta\lambda③} = D_{T③} \cdot \Delta\lambda_{F\leftrightarrow B③}, \tag{10}$$

where ③ denotes the operation period after link calibration. In addition, a thermal coefficient related to the local and remote modules can be included.

### 3.4 Uncertainty budget

To gain a deeper insight into the influence of various factors affecting the calibration of the link, an uncertainty budget has been drawn up as Tab. 1. It is constructed based generally on equation (9), with details given by equations (2), (8) and (10). The uncertainty term related to $\tau_{UTC\to SRC②}$ is excluded from further discussion, as it is an external additive factor that comes from the preceding stage in the case of cascaded links.

The results listed in Tab. 1 show that for short links (50 km to 100 km) the uncertainty of $\Delta\tau_{F\leftrightarrow B②}$ (rows 1 to 7) is dominated by the uncertainty related to measurement of the time interval $\tau_{M②}$ (row 3) that is constant

**Table. 1. Uncertainty budget for the calibration of time transfer fiber link.**

| № | uncertainty source | sensitivity coefficients | | | standard uncertainty | uncertainty contribution | |
|---|---|---|---|---|---|---|---|
| | | | exact form | expanded form | | for 50 km | for 500 km |
| 1 | $\tau^R_{\Delta\lambda①}$ | 0.5× | $\frac{\tau_{M②}}{\tau_{M①}}$ | $\frac{D_② L_②}{D_① L_①}$ | 16.8 ps | 1.4 ps | 14 ps |
| 2 | $\tau_{M①}$ | 0.5× | $\frac{\tau^R_{\Delta\lambda①}\cdot\tau_{M②}}{(\tau_{M①})^2}$ | $\frac{D_② L_②}{D_① L_①}\cdot\frac{\Delta\lambda_{F\leftrightarrow B}}{\Delta\lambda_{FM}}$ | 7 ps | 1.6 ps | 16 ps |
| 3 | $\tau_{M②}$ | 0.5× | $\frac{\tau^R_{\Delta\lambda①}}{\tau_{M①}}$ | $\frac{\Delta\lambda_{F\leftrightarrow B}}{\Delta\lambda_{FM}}$ | 7 ps | 9.3 ps | |
| 4 | $\Delta\lambda_{F\leftrightarrow B②}$ | 0.5× | $\frac{\tau^R_{\Delta\lambda①}}{\Delta\lambda_{F\leftrightarrow B①}}\cdot\frac{\tau_{M②}}{\tau_{M①}}$ | $L_② D_②$ | 1.2 pm | 0.5 ps | 5 ps |
| 5 | $\Delta\lambda_{FM②}$ | 0.5× | $\frac{\tau^R_{\Delta\lambda①}}{\Delta\lambda_{FM①}}\cdot\frac{\tau_{M②}}{\tau_{M①}}$ | $L_② D_②\cdot\frac{\Delta\lambda_{F\leftrightarrow B}}{\Delta\lambda_{FM}}$ | 1.2 pm | 1.35 ps | 13.5 ps |
| 6 | $\tau_S$ | 0.5× | $4\omega A/c^2$ | | $10^{-3}\cdot A_E$ | 0.1 ps | 1 ps |
| 7 | $\tau_B$ | 0.5× | $\sqrt{L}$ | | 0.05 ps/√km | 0.15 ps | 0.5 ps |
| | **uncertainty contribution of rows 1 – 7:** | | | | | **9.5 ps** | **27 ps** |
| 8 | $\tau_{REF\to RET②}$ | 0.5 | | | 7 ps | 3.5 ps | |
| 9 | $\tau_{C①}$ | 0.5 | | | 6.5 ps | 3.25 ps | |
| 10 | $\tau_{SRC\to REF②}$ | 1 | | | 7 ps | 7 ps | |
| 11 | $\tau_{ADV②}$ | 1 | | | 2 ps | 2 ps | |
| 12 | $d\tau/dT$ | 1 | | | 10 ps/√12 | 3.5 ps | |
| | **uncertainty contribution of rows 8 – 12:** | | | | | **9.4 ps** | |
| | **uncertainty contribution of rows 1 – 12:** | | | | | **13.4 ps** | **28.6 ps** |
| 13 | $\Delta\lambda_{F\leftrightarrow B③}$ | 0.5× | $L_②\cdot D$ | | 1.2 pm | 0.5 ps | 5 ps |
| 14 | $\partial D/\partial T$ | 0.5× | $L_②\cdot\Delta T\cdot\Delta\lambda_{F\leftrightarrow B③}$ | | 1.2 fs/(nm·km·K)$^{-1}$ | 0.6 ps | 6 ps |
| | **uncertainty contribution of rows 13 – 14:** | | | | | **0.8 ps** | **7.8 ps** |
| | **total uncertainty (rows 1 – 14):** | | | | | **13.4 ps** | **29.6 ps** |

Comments to lines in the table:

1. Length of calibration fiber $L_①$=300 km assumed.
2. Nominal values of $\Delta\lambda_{F\leftrightarrow B}=0.8\,\text{nm}$ and $\Delta\lambda_{FM}=0.3\,\text{nm}$ assumed.
3. In expanded form, various delays are scaled linearly with appropriate fibers lengths and the differences of lasers wavelength.
4. Both calibration and target fiber assumed to be G.652, with the chromatic dispersion coefficients equal to 17 ps/(nm·km).
5. To include PMD, a link design value (LDV) equal to 0.05 ps/√km is assumed.
6. The fiber is assumed to follow the path along 50th parallel of north latitude. $A_E$ is the area of the projection of the surface swept by a vector extending from the Earth center to the point in the fiber moving in the direction from West to East; ω is the angular speed of the Earth and $c$ is the speed of light in vacuum.

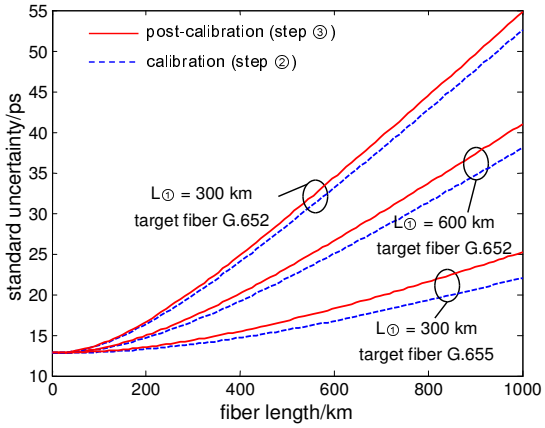


Fig. 5. Standard uncertainty of link calibration versus target fiber length under various conditions. The calibration fiber in all cases is G.652.

and does not scale with the fiber length. For long links, other components start to play a major role and they increase almost equally (rows 1, 2, and 5). The influence of $u\left(\tau^{R}_{\Delta\lambda①}\right)$ and $u\left(\tau_{M①}\right)$ can be reduced simply by increasing the length of the calibration fiber. It is thus generally recommended to use $L_{①}$ of similar (or greater) length as the length of the fiber in the target installation. A reduction of $u\left(\Delta\lambda_{FM②}\right)$ is rather difficult, as it would require substantial improvement of the lasers' stabilization circuitry. Increasing the value of $\Delta\lambda_{FM②}$, although theoretically possible, is difficult in practice because tuning of the wavelength of the laser must consider optical filters that are usually installed just before each optical receiver in ELSTAB to suppress the influence of Rayleigh backscattering. The effects related to Sagnac effect and fiber birefringence (rows 6 and 7, respectively) do not contribute substantially to the combined uncertainty. Entries in rows 8 – 12 collect various uncertainty contributions that are independent of the length of the link that create some noise floor that is significant for short links. Lines 13 and 14 of the table specify the increase of the uncertainty in the period after the link calibration. This contribution is rather small for short links but can become important for very long links.

In Fig. 5, the standard uncertainty of the calibration of time transfer for an individual link, obtained under different conditions (length of the calibration fiber and chromatic dispersion of target fiber), have been plotted. It is evident from these graphs that a very effective method to reduce the calibration uncertainty is to use a fiber with low chromatic dispersion (i.e. ITU-T G.655 instead of G.652) in the target installation. This can be deduced by analyzing Tab. 1 because contributions of $u\left(\tau^{R}_{\Delta\lambda①}\right)$, $u\left(\tau_{M①}\right)$, $u\left(\Delta\lambda_{F\leftrightarrow B②}\right)$ and $u\left(\Delta\lambda_{FM②}\right)$ (rows 1, 2, 4 and 5, respectively) scale linearly with $D_{②}$. This approach is even better than increasing the length of the calibration fiber $L_{①}$ that affects only the contributions of $u\left(\tau^{R}_{\Delta\lambda①}\right)$ and $u\left(\tau_{M①}\right)$.

## 4. Calibration campaigns and results

The calibration of the time transfer of the PoC OTT links was performed two times, during the calibration campaigns in December 2016 and December 2017, respectively. The first campaign was associated with the initial OTT installation, whereas the second one was necessary because of the change of the optical path between the Hannover hub and Bremen (caused by a bridge construction work) and in addition some changes that were applied in the distribution chain of 10 MHz and 1 PPS signals at PTB.

The results of both calibration campaigns are presented in Fig. 6, where the delay relative to UTC(PTB) at the output of each remote module is shown as value inside a rectangle, designated as UTC(PTB) vs. $OUT_x$, where x runs from I to V. These values were obtained using the calibration procedure outlined in Section 3.1 and using the uncertainty estimation method from Section 3.3. To verify the results of the calibration, we took advantage of the fact that at each location the signals traceable to UTC(PTB) are available from two different sources, i.e. UTC(PTB) and output of link IV in Braunschweig, outputs of links I and III in Hannover and outputs of links II and V in Bremen. Because of that, we could perform direct measurements of the differences of 1 PPS signals and compare the results with the values predicted by the calibration. These results are also shown in Fig. 6, placed in the boxes above corresponding locations.

The measurement setup used in both campaigns was similar, however the source of the 10 MHz signal used to synchronize the delay generator (see Section 3.3) was changed. It was a double-oven OCXO (trimmed to UTC(PTB) a day before performing the measurements) in 2016, and a UTC(PTB) signal directly in 2017.

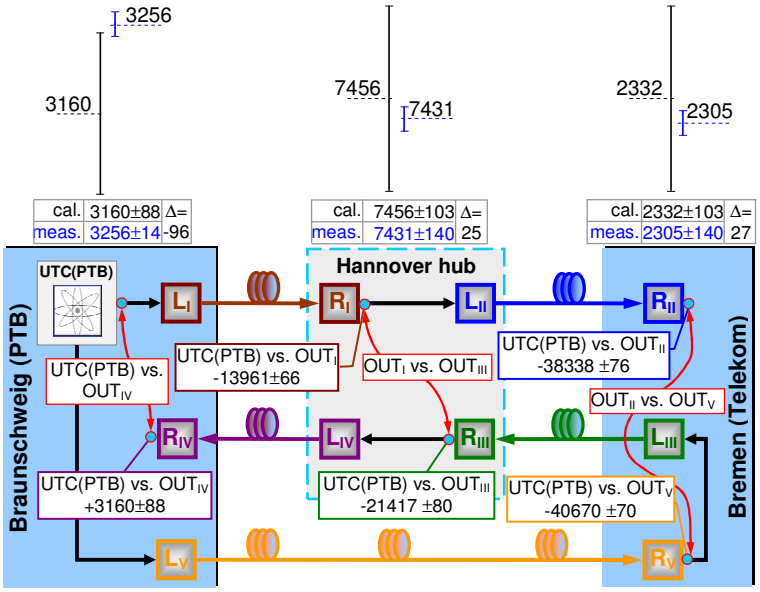


a). calibration campaign 12.2016

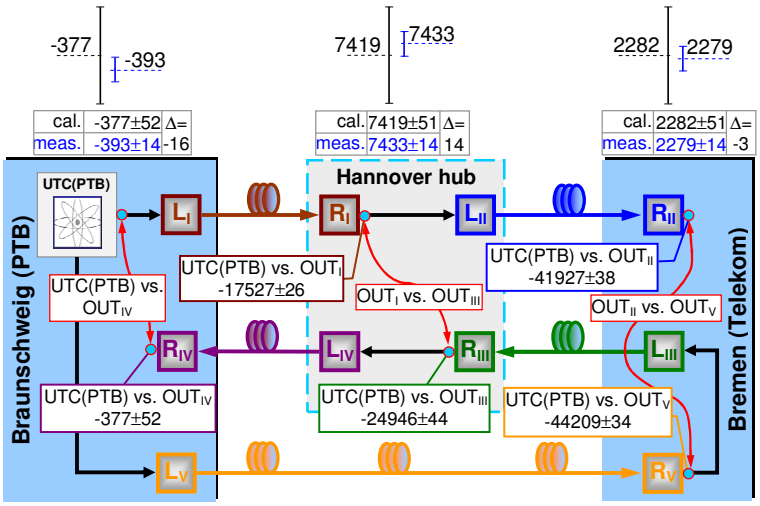


b). calibration campaign 12.2017

Fig. 6. Results of time transfer calibration and its verification. Expanded uncertainty is given as ±2σ, all quantities in ps.

However, a residual difference between OCXO frequency and UTC(PTB) adds error when measuring with the oscilloscope long delays like $\tau_{REF\to RET②}$. In addition, the measurements of $\tau_{SRC\to REF②}$ in links I and V, performed at PTB during the 2016 campaign used a Stanford Research SR620 TIC, which showed a larger uncertainty than assumed when making the uncertainty budget in Section 3.3. When elaborating the data from the 2016 campaign, we thus assumed a standard uncertainty $u(\tau) = 30$ ps for SR620 measurements (that corresponds well to the ±50 ps error included in the product datasheet) and increased the uncertainty associated with the measurement of long delays with the oscilloscope to 10 ps. These are the reasons for ascribing larger uncertainties to the calibration values at the output of the links in 2016.

These differences in the equipment used are probably also responsible for a generally worse agreement between the 1 PPS differences, predicted based on links calibration and obtained from measurements in the 2016 campaign (Fig. 6a). This is visible especially when determining UTC(PTB) vs. $OUT_{IV}$ at PTB and can be explained noting that the measurements performed in Hannover ($OUT_I$ vs. $OUT_{III}$) and Bremen ($OUT_{II}$ vs. $OUT_V$) are influenced by two SR620 measurements that introduce partially correlated systematic errors, which cancel when measuring the difference of two delays. However, only one such measurement is involved at PTB and no further cancellation of systematic errors can occur.

The results from 2017 calibration and verification campaign show very good consistency - the differences between calibration and measurement are well within the uncertainty bounds and do not exceed 16 ps. This is the result of performing all time interval measurements using the oscilloscope and using consequently UTC(PTB)

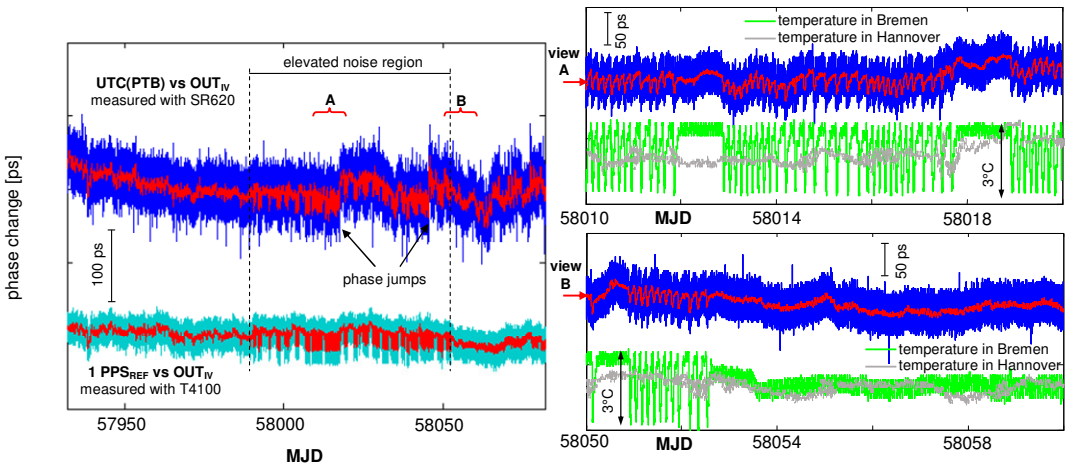


Fig. 7. Fluctuations of 1 PPS signals observed at the output of link IV measured for a period of 150 days (left plot) and expanded part showing correlation of phase fluctuations with temperature in Bremen (right plot). Red overlay is a moving average of 500 consecutive samples.

traceable 10 MHz signal for synchronization of our measurement setup. In this situation, we could probably even decrease the measurement uncertainty related to the time interval to a value below 7 ps.

## 5. Transfer stability

The signals intended for use in the synchronization of telecom infrastructure need to fulfill the requirements concerning their stability, as specified in G.8272 ITU-T recommendations. Assessing the stability in a real link is in general difficult, because the signal at the remote end of the link cannot usually be referred to the input. This is only possible when the transfer link is built as a loop or when signals are delivered to the remote location via two parallel links. As both cases are present in the current OTT architecture we take the opportunity to give subsequently information about the stability of 1 PPS and 10 MHz signals.

### 5.1 Time transfer

The stability of the time transfer was monitored by comparing the 1 PPS output of link IV with UTC(PTB) using a SR620 TIC. These data, affected by fluctuations of the propagation delay of three concatenated links, namely V (Braunschweig-Bremen), III (Bremen-Hannover) and IV (Hannover-Braunschweig) (see Fig. 2) are being collected continuously, starting from the launch of the PoC OTT links in December 2016. Results of a 150-days long period are presented in Fig. 7 (UTC(PTB) vs. $OUT_{IV}$ - blue curve in the left plot) showing a residual phase fluctuation of 19 ps RMS. This plot, however, displays some phase drift in its initial part (before MJD 57970), jumps and periods of elevated noise (between MJD 57990 and 58055), well visible also in averaged data (red overlay curve). To find out the possible reason of such behavior we compared with a second measurement set up in PTB. The 1 $PPS_{OUT}$ of link IV is here compared to 1 $PPS_{REF}$ of link V using a PikTime T4100 TIC. The latter signal is generated inside the local module by dividing the 10 MHz input and initially synchronized with the 1 $PPS_{IN}$. This signal also represents UTC(PTB) but with an offset, and with slightly different pulse shape.

The result of comparison is presented in Fig. 7(left figure, turquoise curve). Both UTC(PTB) vs $OUT_{IV}$ and 1 $PPS_{REF}$ vs $OUT_{IV}$ are similar in terms of periods of elevated noise, although this later one does not display obvious phase drifts or jumps. Apparently, processes inside the SR620 TIC or in the distribution chain of 10 MHz and 1 PPS signals in PTB are responsible for the observed drift and jumps. Noticeably lower noise of the result obtained with T4100 TIC (10 ps vs. 19 ps RMS for T4100 and SR620, respectively) results from its lower internal noise and from the steeper slope of the TIC start signal, UTC(PTB) with about 3 ns rise time and 1 $PPS_{REF}$ with about 0.5 ns rise time.

A closer analysis of the collected data revealed that a strong correlation exists between observed delay fluctuations and temperature fluctuations in Bremen (see right part of Fig. 7). The OTT modules have been installed there in a large server room with large heat generation that is equipped with a relatively poor air-conditioning system, just adequate for operating the telecom equipment. During the same period, the temperature fluctuations in the Hannover hub were at least two-times lower and much slower, so their influence on the phase fluctuations measured in PTB were barely noticeable. The temperature sensitivity of the set of local and remote modules that can be estimated basing on current data is about 10 ps/K and appears to be even lower than known from previous measurements (~16 ps/K) [30], which is probably due tothe improved design of the electronic delay lines currently used inside ELSTAB systems.

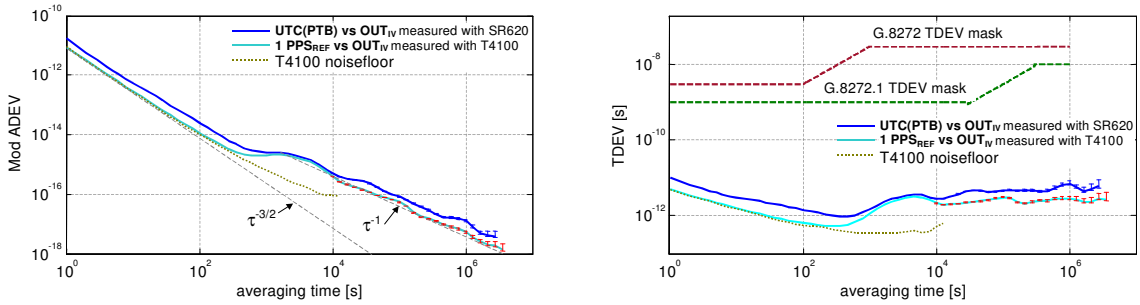


Fig. 8. ModADEV (left plot) and TDEV (right plot) calculated from the data shown in Fig. 7

As a measure of the instability, the modified Allan Deviation (ModADEV) and the time deviation (TDEV) are used. Results for the three concatenated links (V, III and IV) are shown in Fig. 8 for both, SR620 (blue curve), and T4100 (red curve). For averaging times less than a few hundred seconds, ModADEV shows a slope of $\tau^{-3/2}$, characteristic for a white phase noise of the counters used in the measurement (see the noise floor of T4100 also shown in Fig. 8). For longer times, however, the effects caused by the temperature fluctuations in Bremen start to be visible and the slope decreases to $\tau^{-1}$ for $\tau > 2000\,\mathrm{s}$. TDEV stays below 10 ps in the entire observation range (dominated by the TIC noise below a few hundred seconds), showing a tendency to level off for longer times at a few ps level. The stability of the transfer achieved,despite of the effects related to the temperature fluctuations in Bremen,is well below current telecom requirements (see the masks in Fig. 8). The signals delivered by the links are thus of adequate quality for reliable supervision of synchronization equipment like ePRTCs. It is also evident that the long-term stability can be even further improved by improving the air-conditioning in Bremen.

### 5.2 Frequency transfer

So far, we characterized the performance of the concatenated links (I-IV) delivering 10 MHz and 1 PPS signals to Deutsche Telekom Technik, Bremen and back to PTB by comparing the signal received via the fiber link with the local realization of UTC(PTB) using 1 PPS signals and a TIC. We now make use of the second independent fiber link from PTB to Deutsche Telekom Technik GmbH (V) to characterize the performance of the signals at the remote end in Bremen.

As no superior clocks than commercial Cs clocks and only standard counters with resolution at the 10 ps level were available, we decided to set-up a system, depicted in Fig. 8, that allows a direct comparison of the 10 MHz signal provided by the two receiver modules $R_{II}$ and $R_V$ with improved resolution. The system is based on a direct digital synthesizer (DDS) that down-converts the original signals at 10 MHz to the 100 kHz range. This approach is adopted from the well-known Dual Mixer Time Difference (DMTD) method [31]. This signal is subsequently multiplied by a factor *N* using harmonic tracking oscillators that comprise a voltage-controlled oscillator(VCO), a phase-locked loop (PLL), and a divider stage. This system enhances the frequency resolution by a factor of *N*, where *N* is the divider ratio of the frequency divider. For our purpose, the divider ratio was set to *N*=128. The outputs of the two harmonic trackers were counted with a 4-channel dead-time free FXE (K+K Messtechnik GmbH) frequency counter on Ch1 and Ch2 that was referenced to the local Cs clock. In addition to the harmonic signals we also counted the direct outputs provided by the remote modules $R_V$ and $R_{II}$ on Ch3 and Ch4.

Prior to the implementation in Bremen, the measurement equipment was checked at PTB where it showed a noise floor of around 50 fs at short averaging times and temperature sensitivity of about 10 ps/K.For the temperature fluctuations of about 3 K peak-to-peak observed in Bremen (see green curves in Fig. 7) we expect a temperature limited noise floor<30 ps peak-to-peak.

Fig. 9 shows the results obtained over two periods of about three weeks each. It should be noted that the signalsprovided to $R_{II}$ and $R_V$ travel different routes. While the signal for $R_V$ is transferred directly from PTB to Bremen (with amplifiers in between) the signal for $R_{II}$ reaches Bremen via the Hannover hub (including optical to electrical conversion and vice versa, see Fig. 6).

For the data set starting around MJD 58270 the timing noise is significantly smaller as compared to the data starting at MDJ 58107. However, like the measurements discussed previously, the phase difference between the two realizations of the 10 MHz signals show a strong correlation with temperature as already discussed before (Fig. 7).

The corresponding time deviation (TDEV) is shown in Fig. 10. The short-term instability of the 10 MHz signal provided at Bremen is at the level of 100 fs at 1 second measurement time. The TDEV shows a bump around 2000 s that reflects the temperature fluctuations already discussed. A significant improvement of the long-term performance could be obtained (MJD 58270 to MJD 58310) when the measurement equipment was

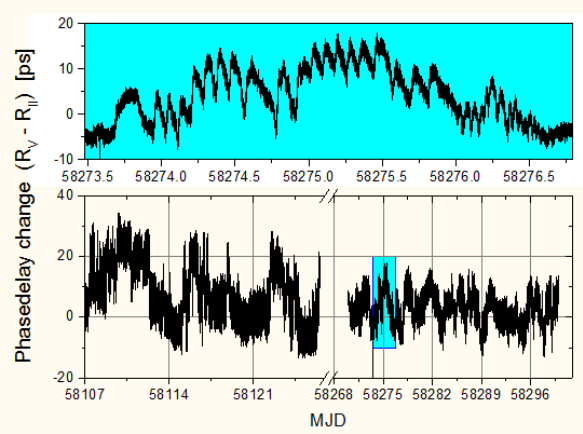


Fig. 9. Phase difference between 10 MHz signals of the receiver modules $R_V$ and $R_{II}$ of the two independent ELSTAB fiber links from PTB to Deutsche Telekom Technik, Bremen. The upper curve shows a zoom of the window indicated by the cyan area in the lower frame.

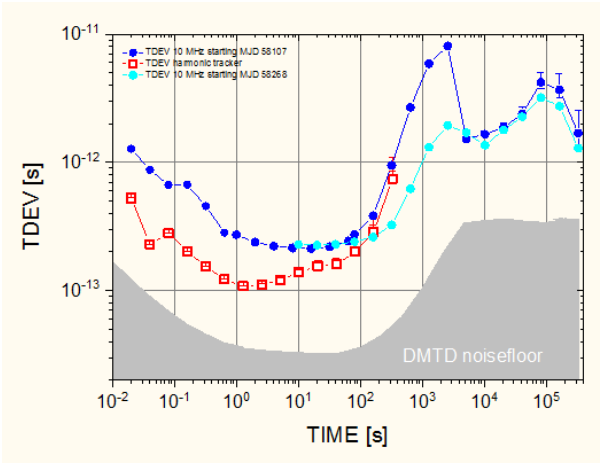


Fig. 10: TDEV calculated from the data shown in Fig. 9.

placed in a rack with front and end doors closed. It should be noted that the TDEV does not exceed values of10 ps for all measurementintervals up to several weeks even in a normal server room with relatively low temperature stability.

Overall, the links are capable to deliver highly stable signals to a remote end with an instability being at least three orders below the current G.8272 requirements. Moreover, the current implementation would allow primary Cs fountain clocks to be compared at the level of their performance that is characterized by an uncertainty at the low $10^{-16}$ level and a frequency instability of the same order of magnitude at one day averaging.

## 6. Conclusion

The links built to test the idea of a supervision of the synchronization in an operationaltelecom network were evaluated several times with respect to delay calibration and time and frequency transfer stability. The technique used to perform a calibration of cascaded links was presented and in-depth analyzed. Calibration of the links as performed and verified in two campaigns showed good consistency within the limits of measurements uncertainty. In particular the second campaign (December 2017) showed that the difference between the measured and predicted propagation delay did not exceed 16 ps ±54 ps.

The stability of the time transfer was evaluated in a loop configuration, where three links were connected in cascade. The measurements performed by comparing UTC(PTB) against its copy(available at the end of the cascaded links) showed a TDEV below 10 ps for the averaging times in the range from 1 s to $>10^6$ s. In the short-term, the stability seems to be limited by the noise of the counters used, however no better counter than widely used SR620 TIC was available to make long-term measurements. In the longer-term ($>10^3$ s) the influence ofthe temperature affecting the end terminals (installed in Braunschweig, Hannover and Bremen) of the individual links start to dominate, mostly because the equipment in Bremen and Hannover is located in large server rooms, with a huge amount of heat generated and an air-conditioning just good enough for standard telecom applications.

To determine the limits of the installed links the measurement of the stability of the frequency delivered to Bremen over two separate links was also undertaken. The measurement setup this time used a DMTD technique with harmonic trackers, showing much lower noise floor than the counters used in previous measurements. The short-term TDEV obtained in these measurements showed values <1 ps, with the minimum of 200 fs for the averaging times in the range of 1 s to 200 s, whereas for longer times once again the influence of temperature in Bremen dominates. As a summary we conclude that the links are capable to deliver highly stable signals to a remote end with an instability being at least two orders of magnitude below the current telecom requirements accordingly to the ITU-T G.8272 recommendation.

## 7. Acknowledgment

We kindly acknowledge receiving funds from the Polish National Science Center under the grants 2014/15/B/ST7/00471 and 2015/17/B/ST7/03628, and from EMPIR initiative co-funded by the European Union's Horizon 2020 research and innovation program and the Participating States via project 15SIB05.

Disclaimer

Commercial products are identified for the sake of technical clarity. No endorsement by the authors or their institutes are implied. We further caution the readers that none of the described equipment's apparent strengths or weaknesses may be characteristic of items currently marketed.

**Appendix: list of used symbols**

| | |
|---|---|
| $\tau_{REF \to OUT}$ | propagation delay between the REF and OUT port |
| $\tau_{REF \to RET}$ | round-trip propagation delay (between REF and RET port) |
| $\tau_{UTC(k) \to SRC}$ | delay between UTC(k) and the local source in cascaded links |
| $\tau_{SRC \to REF}$ | delay between local source and REF port |
| $\tau_{ADV}$ | delay introduced by the 1 PPS advancing block |
| $\tau_C$ | hardware calibration value |
| $\Delta\tau_{F \leftrightarrow B}$ | asymmetry of the optical path of the fiber link |
| $\tau_{\mathrm{S}}$ | asymmetry due to Sagnac effect |
| $\tau_{\mathrm{B}}$ | asymmetry due to fiber birefringence |
| $\tau_{\Delta\lambda}$ | asymmetry due to fiber chromatic dispersion |
| $\lambda_F$ , $\lambda_B$ | optical wavelength of the forward and backward directions |
| $\Delta\lambda_{F \leftrightarrow B}$ | difference of wavelengths between forward and backward directions |
| $D$ , $D_T$ | chromatic dispersion: a per kilometer and accumulated for entire link (total) |
| $\tau^I_{\Delta\lambda}$ | result of indirectly measured asymmetry due to fiber chromatic dispersion |
| $\Delta\lambda_{FM}$ | change of the forward laser wavelength during determining $\tau^I_{\Delta\lambda}$ |
| $\tau_M$ | change of the round-trip delay associated with the change of $\lambda_F$ |
| $\tau^R_{\Delta\lambda}$ | value of fiber asymmetry due to chromatic dispersion required to satisfy eq. (2) |
| $S$ | dispersion slope |
| $\Gamma$ | ratio of required to measured delay asymmetry due to fiber chromatic dispersion |
| ①, ②, ③ | used in superscript to denote in-the-lab pre-calibration, calibration during link installation over the target fiber and period during regular link operation |

**References**


1. ITU-T Recommendation ITU-T G.8271.1/Y.1366.1, "Network limits for time synchronization", Oct. 2017
2. ITU-T Recommendation ITU-T G.8272/Y.1367, "Timing characteristics of primary reference time clocks", Jan. 2015
3. ITU-T Recommendation ITU-T G.8272.1/Y.1367.1, "Timing characteristics of enhanced primary reference time clocks", Nov. 2016
4. Bauch A, Whibberley P 2017 Reliable time from GNSS signals *Inside GNSS*39-44
5. Matsakis D, Levine J, Lombardi M 2018 Metrological and Legal Traceability of Time Signals*Proc. 49th Annual Precise Time and Time Interval Systems and Applications Meeting (Reston, Virginia,USA; January 29 – February 1, 2018)* 59-71
6. Last D 2010 GNSS: the present imperfect *Inside GNSS* **5** 60-64
7. Calonico D, Bertacco E, Calosso C, Clivati C, Costanzo G, Frittelli M, Godone A, Mura A, Poli N, Sutyrin D, Tino G, Zucco M, Levi F 2014 High-accuracy coherent optical frequency transfer over a doubled 642-km fiber link*Appl. Phys. B* **117** 979-986

8. Bercy A, Lopez O, Pottie P Amy-Klein A 2016 Ultrastable optical frequency dissemination on a multi-access fibre network *Appl. Phys B* DOI https://doi.org/10.1007/s00340-016-6463-3
9. Predehl, K. et al. 2012A 920-kilometer optical fiber link for frequency metrology at the 19th decimal place. *Science* **336** 441–444
10. Lopez, O. et al.2015 Frequency and time transfer for metrology and beyond using telecommunication network fibres *C.R. Physique* **16** 531–539
11. Rost M at al. 2012 Time transfer through optical fibers over a distance of 73 km with an uncertainty below 100 ps *Metrologia* **49**772-778
12. Kodet J et al 2016 Two-way time transfer via optical fiber providing subpicosecond precision and high temperature stability*Metrologia* **53** 18
13. Fujieda M, Kumagai M, Gotoh T, Hosokawa M 2009 Ultrastable frequency dissemination via optical fiber at NICT *IEEE Transactions on Instr. and Meas.* **58** 1223-1228
14. Yu L, Wang R, Lu L, Zhu Y, Wu C, Zhang B, Wang P 2014 Stable radio frequency dissemination by simple hybrid frequency modulation scheme *Optics Letters* **39** 5255-5258
15. Chen, X. et al. 2015 Simultaneously precise frequency transfer and time synchronization using feed-forward compensation technique via 120 km fiber link*Sci. Rep.* **5** 18343 doi: 10.1038/srep18343, 2015
16. Schediwy S, Gozzard D, Stobie S, Malan J, Grainge K 2017 Stabilized microwave-frequency transfer using optical phase sensing and actuation*Opt. Lett.* **42** 1648-1651
17. Guéna J, Weyers S, Abgrall M, Grebing C, Gerginov V, Rosenbusch P, Bize S, Lipphardt B, Denker H, Quintin N, Raupach S, Nicolodi D, Stefani F, Chiodo N, Koke S, Kuhl A, Wiotte F, Meynadier F, Camisard E, Chardonnet C, Le Coq Y, Lours M, Santarelli G, Amy-Klein A, Le Targat R, Lopez O, Pottie P, Grosche G 2017 First international comparison of fountain primary frequency standards via a long distance optical fiber link *Metrologia* **54** 348–354
18. Lopez O*at al.* 2013 Simultaneous remote transfer of accurate timing and optical frequency over a public fiber network*Applied Physics B* **110**, 3-6
19. Raupach S, Grosche G2014 Chirped frequency transfer: a tool for synchronization and time transfer *IEEE Trans. Ultrason. Ferroelectr. Freq. Control* **61** 920-929
20. Dierikx E et al 2016 White Rabbit Precision Time Protocol on Long-Distance Fiber Links *IEEE Trans. Ultrason. Ferroelectr. Freq. Control* **63** 945-952
21. Lessing M, Margolis H, Brown C, Marra G 2017 Frequency comb-based time transfer over a 159 km long installed fiber network*Appl. Phys. Lett.* **110** 221101 doi: 10.1063/1.4984144
22. Krehlik P, Śliwczyński Ł, Buczek Ł, Kolodziej J, Lipiński M 2016 ELSTAB- fiber optic time and frequency distribution technology - a general characterization and fundamental limits *IEEE Trans. Ultrason. Ferroel. Freq. Contr.* **63** 993-1004
23. Krehlik P, Śliwczyński Ł, Buczek Ł,Kołodziej J, Lipiński M 2015 Ultrastable long-distance fibre-optic time transfer: active compensation over a wide range of delays*Metrologia* **52** 82–88
24. Śliwczyński Ł, Kołodziej J 2013 Bidirectional optical amplification in long-distance two-way fiber-optic time and frequency transfer systems *IEEE Trans. Instr. Meas.* **62** 253 - 262
25. Jiang Z, Czubla A, Nawrocki J, Lewandowski W, Arias E 2015 Comparing a GPS time link calibration with an optical fibre self-calibration with 200 ps accuracy *Metrologia* **52** 384-391
26. Śliwczyński Ł, Krehlik P, Kolodziej J,Imlau H,Ender H, Schnatz H, Piester D, Bauch A 2017 Fiber-Optic Time Transfer for UTC-Traceable Synchronization for Telecom Networks *IEEE Communications Standards Magazine* **1** 66–73
27. Śliwczyński et al. 2013Dissemination of time and RF frequency via a stabilized fibre optic link over a distance of 420 km *Metrologia* **50** 133–145
28. Krehlik P, Mazur M, Śliwczyński Ł2017 Delay compensation of 1 PPS timetags in fiber-optic time distribution *Proc.2017 Joint Conference of the European Frequency and Time Forum and IEEE International Frequency Control Symposium* (*Besancon; France; July 9-13, 2017*) 366-367
29. Krehlik P, Śliwczyński Ł 2016 Fiber-optic time distribution with the autonomous calibration of dispersion-induced offset *Proc. 2016 European Frequency and Time Forum* (*York, UK, April 4-7, 2016*) DOI: 10.1109/EFTF.2016.7477760
30. Barnes C, Hati A, Nelson C, Howe D 2016 Practical evaluation of a 50 km fiber link utilizing a commercial modem *Proc. 2016 IEEE International Frequency Control Symposium* (*New Orleans, USA, May 9-12, 2016*) 1-4

31. S. R. Stein Frequency and Time - Their Measurement and Characterization, Chapter 12, pp.191-416, *Precision Frequency Control*, Vol. 2, Edited by E.A. Gerber and A. Ballato, Academic Press, New York, 1985, ISBN 0-12-280602-6